Scientia Iranica B (2018) 25(3), 1303–1311

SCIENTIA IRANICA

Sharif University of Technology
Scientia Iranica
Transactions B: Mechanical Engineering
http://scientiairanica.sharif.edu

Research Note

A note on the critical gap of bubble coalescence during foaming process: Diffuse-interface modeling

E. Amiri Rad*

Department of Mechanical Engineering, Hakim Sabzevari University, P.O. Box 397, Iran

Received 27 July 2016; received in revised form 21 February 2017; accepted 1 May 2017

KEYWORDS
Bubble;
Coalescence;
Critical gap;
Foaming;
Lattice Boltzmann.

Abstract. Bubble coalescence is an important stage of foaming process. A goal of foaming is to produce numerous, uniform-size bubbles. Therefore, suppression of bubble coalescence is desirable during foaming process. For stationary bubbles, if their distance is less than a critical gap, they will coalesce. Actually, in this case, attractive forces attract the outer surfaces to touch each other and form a growing gas bridge, which finally merges the bubbles. For bigger distance, the attractive forces cannot make a bridge and coalescence will not happen. In this study, the dynamics of bubble coalescence are modeled using a diffuse-interface LBM. Then, critical gap of bubble coalescence is defined as the maximum distance between the stationary bubbles where the coalescence will happen. Sensibility of critical gap is obtained with respect to critical properties of material, bubble size, viscosity of gas and liquid, density ratio, surface tension, temperature, and interface thickness. The results show that interface thickness is the only factor that controls the critical gap. In other words, in the case of stationary bubbles, by a precise estimation of interface thickness, the coalescence can be predicted. Critical gap is a useful parameter in foaming where the maximum number of bubbles is desirable.

1. Introduction

Foaming is a complex process in multiphase systems that has important applications in the food and chemical industries, firefighting, mineral processing, and structural material science and has considerably attracted interest of the researchers [1-8]. Foaming consists of 3 stages, namely, nucleation, bubble growth, and coarsening. During the coarsening stage, formed bubbles coalesce and combine with larger bubbles. The bubble and droplet coalescence has been addressed by many researchers via experimental or numerical studies [9-34].

*. *Tel/Fax: +98 5144012521;*
E-mail address: a.amirirad@hsu.ac.ir

doi: 10.24200/sci.2017.4335

Bubble coalescence is mainly explained by two theories. The first one is film drainage theory, which considers the time required for the drainage of the thin liquid between two bubbles. Actually, the interfacial forces, such as van der Waals attractive force, cause the drainage of liquid film. The details of this theory have been discussed by Chaudhari and Hofmann [30]. The second theory is stochastic theory, which was proposed in 2002 by Ghosh and Juvekar for coalescence of drops and bubbles [25]. Paulsen et al. used an electrical method and high-speed imaging to describe the droplets coalescence. They showed that the outer fluid had a small effect on the coalescence dynamics [9-12].

Baroudi et al. investigated the growth dynamics of the connecting liquid bridge during the coalescence of two droplets in a binary system using LBM [13]. Sprittles simulated coalescence numerically and com-

pared the results with experimental data [14]. Czerski investigated sound during bubble coalescence [15]. Case et al. employed an electrical method to study the coalescence of two low-viscosity droplets at early times [16,17]. Aryafar et al. used an ultrafast x-ray phase-contrast imaging to investigate the early merging dynamics of two water drops in air [18]. Giribabu and Ghosh developed an experimental technique for studying coalescence where two bubbles were allowed to rest together in a conical cell, which was immersed in an aqueous surfactant solution [19]. They focused on the interfacial dynamics after two bubbles touched.

Gilet et al. experimentally investigated the partial coalescence of a droplet on a planar liquid/liquid interface for various viscosity ratios [20]. Dirk et al. studied droplet coalescence in a molecular system for different viscosities and an ultralow surface tension [21]. Thoroddsen et al. used an ultra-high-speed video camera to study the coalescence for different drop sizes and liquid viscosities [22]. Duchemin et al. studied the coalescence of two droplets where they assumed approach velocity of zero and neglected the dynamical effects of the outer fluid. They found that the minimum radius of the connecting bridge was proportional to square root of time [23]. Wu et al. used a high-speed imaging system to investigate the coalescence of two liquid drops driven by surface tension [24]. Their experimental results confirmed the scaling law that was proposed by Duchemin. Eggers et al. simulated coalescence with an external viscous fluid both analytically and numerically [26]. Stover et al. used both FEM and experimental methods to study small bubble coalescence [28].

The bubble coalescence is governed by interaction forces between the bubbles. When two bubbles are at rest beside each other, there are some attractive and repulsive forces between their interfaces. When attractive forces overcome the repulsive forces and inertia of the droplets, the bubbles will certainly coalesce. The main attractive force is van der Waals, which is responsible for coalescence.

The van der Waals force between the bubbles is inversely proportional to the distance between their interfaces. Therefore, the closer the bubbles, the higher the van der Waals force would be, which makes coalescence easier. When they are farther, the van der Waals force is not strong enough to attract them and cause coalescence. Eventually, there should be a critical distance between the bubbles.

The desirable foaming process occurs when there are numerous, equal-size bubbles. This means that avoiding or postponement of coalescence is a favor. However, even in a static system without bubble motion and collision, when the distance between interfaces is less than a minimum value (critical gap), van der Waals attractive forces may push the neighbor bubbles toward each other to coalesce. If the bubbles stand far away adequately and their distance is greater than the mentioned critical gap, they will not coalesce and this is desirable in foaming process. The objective of this paper is simulation of coalescence stage of foaming and investigating the critical gap between the bubbles.

Conventionally, the interface of gas and liquid is assumed infinitely thin where the physical properties are discontinuous. Obviously, coalescence is governed by the interface dynamics of a gas-liquid system and cannot be handled by such a sharp-interface model. Therefore, a diffuse-interface model is used that simplifies the treatment of the interface. Here, the fluid properties change smoothly across the interface layer. A diffuse-interface model also considers the morphological variations of interfaces much more easily than a sharp-interface description does.

Lattice Boltzmann method is considerably efficient for simulating interface dynamics [35-45]. Regarding the thermodynamic treatment of the free energy, i.e. the use of a van der Waals fluid model, the behavior of bubble interfaces in the free-energy LBM can be related to van der Waals forces [42,43]. This is an important advantage over similar methods in which a specified length or the grid resolution governs the occurrence of coalescence.

In this paper, a van der Waals-based free energy LBM is used for modeling a gas-liquid system. Using the developed model, coalescence process of 2 stationary equal-size bubbles in a static bulk liquid is modeled; consequently, critical gap of coalescence and its dependency on the important parameters of the system are studied.

2. Simulation method

Lattice Boltzmann equation with a single relaxation time parameter can be expressed as the following [46]:

$$f_i(\vec{r}+\vec{c}_i\Delta t, t+\Delta t) = \left(1-\frac{1}{\tau_f}\right) f_i(\vec{r},t) + \frac{1}{\tau_f} f_i^0(\vec{r},t), \quad (1)$$

where $\vec{r}$ is the lattice position vector, $\vec{c}_i$ is particle velocity, t is time, τ_f is the single relaxation time parameter, $f_i(\vec{r},t)$ denotes the particle distribution associated with the discrete velocity $\vec{c}_i$, and f_i^0 indicates the local equilibrium distribution function. The discrete velocity $\vec{c}_i$ is chosen, such that $\vec{c}_i\Delta t$ is a lattice vector. In this paper, a two-dimensional square lattice with 9 velocity vectors (D2Q9 Lattice) is used.

Using a suitable equilibrium distribution function, Eq. (1) can describe continuity and Navier-Stokes equations for a non-ideal, one-component fluid [41]. Hydrodynamic parameters of the flow are related to distribution function as follows:

$$\rho = \sum_i f_i, \quad (2)$$

$$\rho u_j = \sum_i f_i c_{ij}, \tag{3}$$

where ρ is fluid density and u_j is flow velocity vector. The key point in simulating non-ideal, two-phase flow by LBM is finding a suitable equilibrium distribution function that describes the thermodynamic behavior of this flow. Equilibrium distribution function can be considered as a second order expansion of velocity:

$$f_i^0 = A + Bu_j c_{ij} + CU^2 + Du_j u_k c_{ij} c_{ik} + G_{jk} c_{ij} c_{ik}. \tag{4}$$

Regarding the conservation of Eqs. (2) and (3), the zeroth and first moments of equilibrium distribution function are as the following:

$$\sum_i f_i^0 = \rho, \quad \sum_i f_i^0 c_{ij} = \rho u_j. \tag{5}$$

The next moment is chosen such that the continuum macroscopic equations correctly describe the hydrodynamics of a one-component, non-ideal fluid. This gives [40]:

$$\sum_i f_i^0 c_{ij} c_{ik} = P_{jk} + \rho u_j u_k + \upsilon \left(u_j \frac{\partial \rho}{\partial x_k} + u_k \frac{\partial \rho}{\partial x_j} + \delta_{jk} u_m \frac{\partial \rho}{\partial x_m} \right). \tag{6}$$

P_{jk} is the pressure tensor and υ is kinematic viscosity. The first formulation of the model omits the third term in Eq. (6) and is not Galilean invariant. Holdych et al. showed that the addition of this term led any non-Galilean invariant terms to be of the same order as finite lattice corrections to the Navier-Stokes equations [47]. In order to fully constrain the coefficients, a fourth condition is needed, which is [44]:

$$\sum_i f_i^0 c_{ij} c_{ik} c_{im} = \frac{\rho c^2}{3} (u_j \delta_{km} + u_k \delta_{jm} + u_m \delta_{jk}). \tag{7}$$

The pressure tensor can be defined as [48]:

$$P_{ij} = p(\vec{x}) \delta_{ij} + \lambda \left(\frac{\partial \rho}{\partial x_i} \right) \left(\frac{\partial \rho}{\partial x_j} \right), \tag{8}$$

where λ is capillary coefficient and $p(\vec{x})$ is:

$$p(\vec{x}) = p_0 - \lambda \rho \nabla^2 \rho - \frac{\lambda}{2} |\partial_\alpha \rho|^2. \tag{9}$$

Also, p_0 is obtained using equation of state as:

$$p_0 = \rho \psi' - \psi, \tag{10}$$

where ψ is the bulk free energy density as the following [41]:

$$\psi = p_c (\alpha + 1)^2 (\alpha^2 - 2\alpha + 3 - 2\beta\tau). \tag{11}$$

Here, β is compressibility constant; $\alpha = \frac{\rho}{\rho_c} - 1$ is the non-dimensional density; $\tau = 1 - \frac{T}{T_c}$ is the non-dimensional temperature; and T_c, p_c, and ρ_c are the critical temperature, critical pressure, and critical density, respectively.

Landau defined the total free energy of a two-phase system as a composite of bulk and interfacial parts as follows [49]:

$$\Psi = \int \left(\psi(T, \rho) + \frac{\lambda}{2} |\partial_\alpha \rho|^2 \right) dV. \tag{12}$$

This function can describe the equilibrium properties of a one-component, two-phase fluid. Obviously, pressure is the connector between free energy function and LBM algorithm.

Subscribing Eq. (4) in Relations (5), (6), and (7), the unknown coefficients of equilibrium distribution function can be found and equilibrium distribution function of a two-phase system can be thoroughly determined [38].

The analysis of Holdych et al. showed that Eq. (1) approximated the continuity as follows:

$$\frac{\partial \rho}{\partial t} + \nabla . \rho \vec{u}. \tag{13}$$

Also, Navier-Stokes equations can be recovered in low Mach numbers as follows [41]:

$$\frac{\partial \rho u_i}{\partial t} + \frac{\partial \rho u_i u_j}{\partial x_j} = -\frac{\partial P_{ij}}{\partial x_j} + \upsilon \frac{\partial}{\partial x_j} \left(\rho \left\{ \frac{\partial u_i}{\partial x_j} + \frac{\partial u_j}{\partial x_i} + \delta_{ij} \frac{\partial u_k}{\partial x_k} \right\} \right) - \frac{3\upsilon}{c^2} \frac{\partial}{\partial x_j} \left(u_i \frac{\partial P_{jk}}{\partial x_k} + u_j \frac{\partial P_{ik}}{\partial x_k} + \frac{\partial}{\partial x_k} (\rho u_i u_j u_k) \right). \tag{14}$$

Therefore, the solution to Lattice Boltzmann equation will lead to continuity and Navier-Stocks solution in low Mach numbers.

In original free energy method, the same relaxation time parameter is used for both liquid and vapor [42,43]. In this situation, the model cannot cover different kinematic viscosity ratios. Therefore, a local relaxation time parameter is introduced to overcome this problem. In this method, 2 different relaxation time parameters are defined for liquid and vapor, and local relaxation time parameter is found by a linear interpolation between them as follows [37]:

$$\tau_f = \frac{\tau_g - \tau_l}{\rho_g - \rho_l} \times (\rho - \rho_l) + \tau_l. \tag{15}$$

Subscribes g and l refer to vapor and liquid, respectively, and ρ is local density of the flow. By local definition of relaxation parameter, kinematic viscosity can be differently defined for liquid (υ_l) and vapor (υ_g).

3. Results and discussion

3.1. Interface thickness

Interface thickness is a consequence of the diffuse-interface model and its accurate estimation has important role in valid modeling. Interface thickness of such a gas-liquid system can be theoretically given by [41]:

$$h = \sqrt{\frac{\lambda \rho_c^2}{4 p_c \beta \tau}}. \tag{16}$$

In a gas-liquid system, the main physical variable, which distinguishes the phases, is density that gradually varies across the interface. To check the validity of the simulation, a planar interface is implemented in a 150 × 100 grid size for critical properties of $p_c = 0.125$, and $p_c = 3.5$. Using the equilibrium density profile obtained by the developed diffuse-interface model, interface thickness can be numerically estimated. Different cases of v_g, v_l, λ, and $\beta\tau$ are chosen and interface thickness is found theoretically and numerically as shown in Table 1. Also, the effects of bubble radius on the interface thickness are shown in Table 2.

Based on the results of Tables 1 and 2, the developed model can capture the interface thickness precisely and its error is almost negligible.

Table 1. Numerical and theoretical interface thicknesses for planar geometry ($p_c = 0.125$, and $\rho_c = 3.5$).

λ	$\beta\tau$	v_l	v_g	h_{th}	h_{LBM}	Error (%)
0.015	0.03	0.167	0.167	3.5	3.3691	3.7
	0.1			1.917	1.9356	1.0
	0.3			1.1068	1.0914	1.4
	0.4			0.9585	0.9557	0.3
0.020				1.1068	1.0906	1.5
0.025				1.2374	1.1996	3.1
0.015		0.267	0.267	0.9585	0.9536	0.5
		0.383	0.383	0.9585	0.9655	0.7
		0.5	0.5	0.9585	0.9558	0.3
			0.333	0.9585	0.9505	0.8
			0.167	0.9585	0.9535	0.5

3.2. Surface excess energy

Surface excess energy is the concentrated energy at the interface that is interpreted as the surface tension. The expression for the surface excess energy of a van der Waals fluid at equilibrium is found to be [50]:

$$\sigma = \int_0^\infty \lambda \left(\frac{d\rho}{d\eta}\right)^2 d\eta. \tag{17}$$

Therefore, by the density profile obtained from the diffuse-interface model, the excess free energy of the interface can be found numerically.

On the other side, surface excess energy can be theoretically derived by the following formula [41]:

$$\sigma_{th} = \frac{4}{3}\rho_c \sqrt{2(\beta\tau)^3 \lambda\, p_c}. \tag{18}$$

A central bubble is considered in a 150 × 100 grid size with critical properties of $p_c = 0.125$, and $p_c = 3.5$. To check the accuracy of the results, theoretical and numerical values of surface excess energy are tabulated for different cases of bubble radius and thermophysical properties in Table 3.

Based on the results, the error of numerical surface excess energy, in comparison with the theoretical one, is less than 2%, which is almost negligible.

3.3. Grid dependency

Grid size is defined as a function of the bubble radius ($6R \times 4R$). The sizes of the grids used in this analysis are 150 × 100 ($R = 25$), 300 × 200 ($R = 50$), 450 × 300 ($R = 75$), and 600 × 400 ($R = 100$). The effects of grid resolution on the surface tension and interface thickness are shown in Table 4.

Based on the results, using the 150 × 100 grid size would provide reasonable accuracy and avoid high computational costs.

Table 3. Numerical and theoretical surface excess energy ($p_c = 0.125$, and $\rho_c = 3.5$).

R	λ	$\beta\tau$	σ_{th}	σ_{LBM}	Error (%)
25	0.01	0.03	0.00121	0.00120	1.17
30	0.015	0.1	0.00904	0.00906	0.21
35	0.02	0.2	0.02951	0.02977	0.85
40	0.025	0.3	0.06062	0.06141	1.29

Table 2. Numerical and theoretical interface thicknesses for different radiuses ($p_c = 0.125$, and $\rho_c = 3.5$).

R	λ	$\beta\tau$	v_l	v_g	h_{th}	h_{LBM}	Error (%)
Planar	0.015	0.4	0.167	0.167	0.9585	0.9557	0.3
40						0.9558	0.3
30						0.9655	0.7
25						0.9368	2.3

Table 4. Effects of grid size on the accuracy of model ($p_c = 0.125$, $\rho_c = 3.5$, $\beta\tau = 0.4$, and $\lambda = 0.035$).

R	N_x	N_y	σ_{th}	σ_{LBM}	Error of σ (%)	h_{th}	h_{LBM}	Error of h (%)
25	150	100	0.11043	0.11184	1.28	1.4642	1.4294	2.4
50	300	200		0.11199	1.41		1.4147	3.4
75	450	300		0.11201	1.42		1.4163	3.3
100	600	400		0.11199	1.41		1.4235	2.8

3.4. Order of convergence

Order of convergence of the scheme with respect to surface tension can be obtained as follows:

$$\lim_{n\to\infty} \frac{\left|\sigma_{n+1} - \sigma\right|}{\left|\sigma_n - \sigma\right|} = \gamma. \tag{19}$$

This means that for large iterations, the surface tension converges to 'σ' with order of convergence of γ. The value of γ is called the asymptotic error constant.

For different grids in Table 4, the order of convergence is found after 3000 iterations as shown in Table 5.

Obviously, for all of them, the sequence converges linearly with the order of 1.

3.5. Critical gap of bubble coalescence

In this Section, 2 initially stationary equal-size bubbles with radius of (R) are suspended in static liquid, while the distance between their outer boundaries is (W). The schematic configuration of the problem is shown in Figure 1.

In the case of small distances between the bubble boundaries, van der Waals attractive forces are in the order that they can move the bubble surfaces toward each other, make a bridge, and cause coalescence as Figure 2 shows. But, if their distance is greater than a critical value–it is named critical gap (W_{cr}) in this paper–van der Waals attractive forces are not as big as they can make bubble coalescence. In the following, the effects of different parameters on the critical gap of bubble coalescence are investigated.

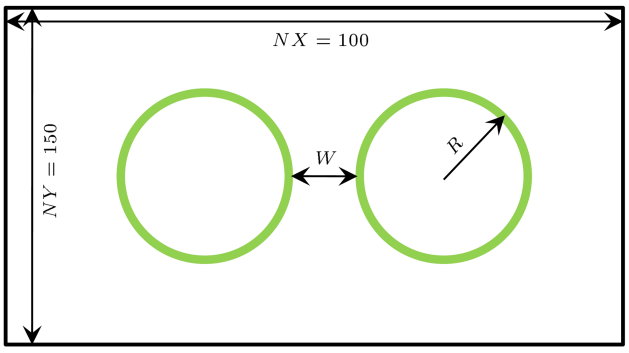

Figure 1. Schematic configuration of initial conditions of the problem.

Table 5. Order of convergence of the model ($p_c = 0.125$, $\rho_c = 3.5$, $\beta\tau = 0.4$, and $\lambda = 0.035$).

R	N_x	N_y	Order of convergence	Asymptotic error constant
25	150	100	1	1
50	300	200	1	1
75	450	300	1	1
100	600	400	1	1

3.5.1. Effects of bubble radius

One parameter that may affect the coalescence process is bubble size. In order to find the sensibility of critical gap against bubble diameter, the critical gap of coalescence is obtained for different radii in the case of $p_c = 0.125$, $\rho_c = 3.5$, $\beta\tau = 0.4$, and $\lambda = 0.035$. The critical gap of coalescence is found almost the same for all test cases of different radii, with a standard deviation of 1.53%. Therefore, occurrence or non-occurrence of coalescence is independent from bubble radius, and bubble size does not have any influences on the critical gap of coalescence.

3.5.2. Effects of relaxation time parameter

Relaxation time parameter is a key factor in LBM simulation that also governs kinematic viscosity. By local definition of time relaxation parameter, kinematic viscosity can be defined differently for liquid and vapor. The critical gap of coalescence is found almost the same for different time relaxation parameters (kinematic viscosity) of gas in the case of constant time relaxation parameter (kinematic viscosity) of liquid with a standard deviation of 0.01%.

In the next step, time relaxation parameter (kinematic viscosity) of gas is fixed and critical gap of coalescence is found for different values of time relaxation parameter (kinematic viscosity) of liquid. In this case, the standard deviation is 1.3%. Based on the results, critical gap of coalescence is independent of time relaxation parameter. Therefore, kinematic viscosity will not affect the critical gap of coalescence. The independency of results from time relaxation parameter also confirms the accuracy and reliability of LBM model.

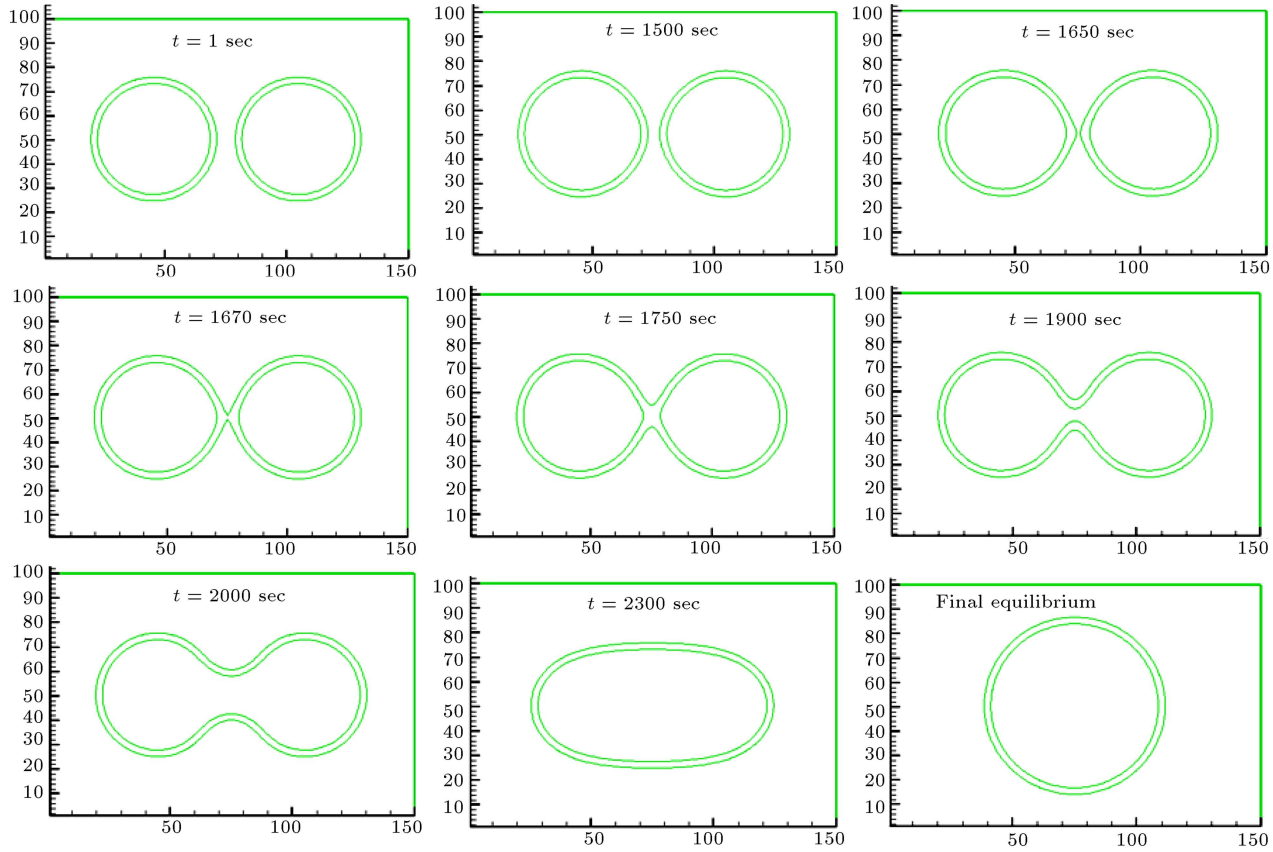

Figure 2. A typical coalescence process of initially stationary bubbles.

3.5.3. Effects of capillary coefficient and $\beta\tau$

$\beta\tau$ and λ are two governing parameters in this simulation; they control the interface thickness and surface tension as in Eqs. (16) and (18). Also, the density ratio is governed by $\beta\tau$ as follows:

$$\frac{\rho_l}{\rho_g} = \frac{1+\sqrt{\beta\tau}}{1-\sqrt{\beta\tau}}. \tag{20}$$

In the first step, variations of critical gap with $\beta\tau$ in the case of constant λ are obtained (Case 1). Then, $\beta\tau$ is fixed and λ is changed step by step (Case 2). In these two cases, critical gap of coalescence varies with surface tension and interface thickness. Figure 3 shows the effects of surface tension in Cases 1 and 2. Based on the results, surface tension has an opposite influence on the critical gap of coalescence in the cases of $\beta\tau$ and λ variations. Similarly, the effects of interface thickness on the critical gap are plotted in Figure 4.

Critical gap of coalescence increases almost linearly with interface thickness in both cases of $\beta\tau$ and λ variations. Here, one can conclude that interface thickness governs the parameter of critical gap of coalescence. To get a better understanding of the problem, interface thickness is fixed by variations of $\beta\tau$ and λ as in Table 6.

In the case of constant interface thickness, critical gap of coalescence is found for different surface

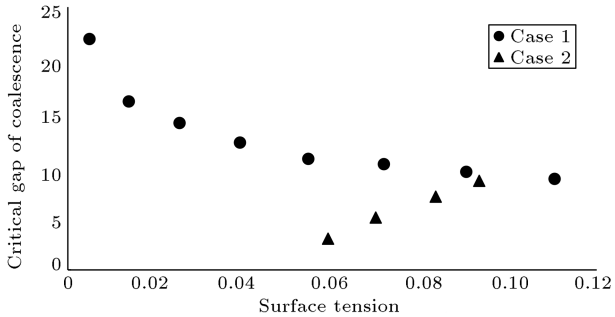

Figure 3. Variations of critical gap of bubble coalescence against surface tension in Case 1 ($\lambda = 0.035$), and Case 2 ($\beta\tau = 0.4$).

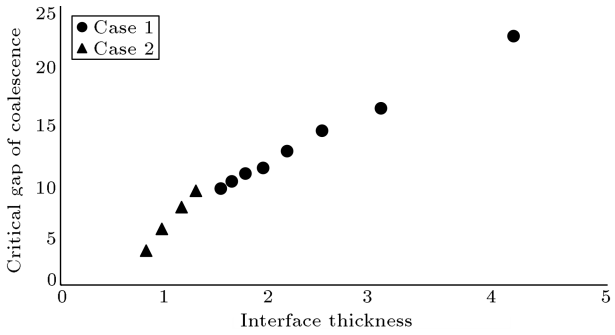

Figure 4. Variations of critical gap of bubble coalescence against interface thickness in Case 1 ($\lambda = 0.035$), and Case 2 ($\beta\tau = 0.4$).

Table 6. Different choices of λ and $\beta\tau$ with constant interface thickness ($p_c = 0.125$, and $\rho_c = 3.5$).

λ	$\beta\tau$	ρ_l/ρ_g	σ	h	Averaged critical gap ($\bar{W}_{cr}$)
0.035	0.4	4.44	0.11043		
0.03	0.34	3.8	0.08113		
0.025	0.29	3.33	0.05634	1.4642	8.9
0.02	0.23	2.84	0.03606		
0.015	0.17	2.4	0.02028		

Table 7. Different choices of p_c and ρ_c with constant interface thickness ($\lambda = 0.035$ and $\beta\tau = 0.4$).

P_c	ρ_c	σ	h	Averaged critical gap ($\bar{W}_{cr}$)
0.13	3.57	0.11485		
0.125	3.5	0.11043		
0.12	3.43	0.10602		
0.11	3.28	0.09718	1.4642	8.9
0.1	3.13	0.08835		
0.08	2.8	0.07068		
0.05	2.21	0.04417		

tensions and standard deviation is calculated at 1.4%. Therefore, critical gap of coalescence is independent of surface tension while it is influenced by interface thickness.

3.5.4. Effects of critical properties

It is shown that in the case of constant critical pressure and density, interface thickness is the only governing factor of critical gap of coalescence. But, interface thickness also varies with critical properties. Several cases of critical density and pressure are chosen as in Table 7 where the interface thickness is constant.

In this case, the standard deviation is 1.16% and constant interface thickness leads to constant critical gap of coalescence.

3.5.5. Effects of interface thickness

It is concluded that for different values of body size, surface tension, density ratio, and kinematic and dynamic viscosity as well as for different materials, the critical gap of coalescence is only a function of interface thickness. Therefore, regardless of the other parameters, critical gap of coalescence can be estimated by calculating interface thickness. Critical gap of coalescence has been found for many cases of interface thickness and the results are plotted in Figure 5. Based on the results, critical gap of coalescence has a linear relation with interface thickness.

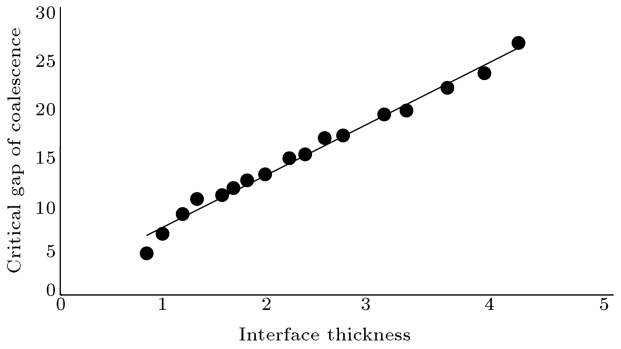

Figure 5. Variations of critical gap of bubble coalescence against interface thickness.

4. Summary and conclusions

A gas-liquid system was modeled by a diffuse-interface free energy LBM. To check the accuracy of the model, interface thickness and surface tension of a single bubble were found where the error was negligible (3Tables 1-3). After a grid resolution analysis, the coalescence stage of foaming process was simulated for 2 initially stationary bubbles and critical gap of coalescence was obtained for them. In the absence of any initial motion of bubbles or bulk liquid, when the bubbles were not in contact, but were very close, they coalesced. Actually, when the gap between their outer boundaries was less than a critical gap, their surfaces were attracted to each other to shape a bridge, which grew and caused coalescence as in Figure 2. The critical gap of coalescence was a useful parameter that helped us to determine the least distance between the bubbles to avoid coalescence. Sensibility of this critical gap was evaluated with respect to many parameters such as critical properties of the material, density ratio, kinematic viscosity of liquid and vapor, bubble radius, surface tension, temperature, and interface thickness. The results showed that critical gap of coalescence was only a function of interface thickness as shown in Figure 5. In fact, for different materials with various radii and thermophysical properties, if the interface thickness was calculated precisely, the critical gap of coalescence could be estimated.

References

1. Malekjafarian, M. and Sadrnezhaad, S.K. "Effect of SiC on microstructural features and compressive properties of aluminum foam", *Scientia Iranica*, **21**(4), pp. 1325-1329 (2014).
2. Latifizadeh, H. "An analytical method to analysis of foam drainage problem", *International Journal of Mathematical Sciences*, **7**(1), (2013).
3. Feng, J.J. and Bertelo, C.A. "Prediction of bubble growth and size distribution in polymer foaming based on a new heterogeneous nucleation model", *J. Rheol.*, **48**, pp. 439-462 (2004).

4. Hilgenfeldt, S., Koehler, S.A., and Stone, H.A. "Dynamics of coarsening foams: Accelerated and self-limiting drainage", *Phys. Rev. Lett.*, **86**(20), pp. 4704-4707 (2001).
5. Sandler, J., Wollecke, F., Altstadt, V., Wettstein, E., and Rakutt, D. "Principal correlation of pvc melt elongational properties with foam cell morphology", *Cellular Polym.*, **19**, pp. 371-388 (2000).
6. Shafi, M.A. and Flumerfelt, R.W. "Initial bubble growth in polymer foam processes", *Chem. Eng. Sci.*, **52**, pp. 627-633 (1997).
7. Ramesh, N.S., Rasmussen, D.H., and Campbell, G.A. "The heterogeneous nucleation of microcellular foams assisted by the survival of microvoids in polymers containing low glass transition particles. Part i: mathematical modeling and numerical simulation", *Polym. Eng. Sci.*, **34**, pp. 1685-1696 (1994).
8. Arefmanesh, A., Advani, S.G., and Michaelides, E.E. "A numerical study of bubble growth during low pressure structural foam molding process", *Polymer Eng. Sci.*, **30**, pp. 1330-1337 (1990).
9. Paulsen, J.D., Carmigniani, R., Kannan, A., Burton, J.C., and Nagel, S.R. "Coalescence of bubbles and drops in an outer fluid", *Nat. Commun.*, **5**(3182) (2014). Doi: 10.1038/ncomms4182.
10. Paulsen, J.D. "Approach and coalescence of liquid drops in air", *Phys. Rev. E.*, **88**, 063010 (2013).
11. Paulsen, J.D., Burton, J.C., Nagel, S.R., Appathurai, S., Harris, M.T., and Basaran, O.A. "The inexorable resistance of inertia determines the initial regime of drop coalescence", *Proc. Natl. Acad. Sci.* USA., **109**, pp. 6857-6861 (2012).
12. Paulsen, J.D., Burton J.C., and Nagel, S.R. "Viscous to inertial crossover in liquid drop coalescence", *Phys. Rev. Lett.*, **106**, 114501 (2011).
13. Baroudi, L., Kawaji, M., and Lee T. "Effects of initial conditions on the simulation of inertial coalescence of two drops", *Comp. Math. Appl.*, **67**, pp. 282-289 (2013).
14. Sprittles, J.E. and Shikhmurzaev, Y.D. "Coalescence of liquid drops: Different models versus experiment", Phys. Fluids, **24**, 122105 (2012).
15. Czerski, H. "A candidate mechanism for exciting sound during bubble coalescence", *J. Acoust. Soc. Am.,* **129**, EL83-EL88 (2011).
16. Case, S.C. "Coalescence of low-viscosity fluids in air", *Phys. Rev. E.*, **79**, 026307 (2009).
17. Case, S.C. and Nagel, S.R. "Coalescence in low-viscosity liquids", *Phys. Rev. Lett.*, **100**, 084503 (2008).
18. Fezzaa, K., and Wang, Y. "Ultrafast x-ray phase-contrast imaging of the initial coalescence phase of two water droplets.", *Phys. Rev. Lett.*, **100**, 104501 (2008).
19. Giribabu, K. and Ghosh, P. "Binary coalescence of air bubbles in viscous liquids in presence of non-ionic surfactant", *Can. J. Chem. Eng.*, **86**, pp. 643-650 (2008).
20. Gilet, T., Mulleners, K., Lecomte, J.P., Vandewalle, N., and Dorbolo, S. "Critical parameters for the partial coalescence of a droplet", *Phys. Rev. E.*, **75**, 036303 (2007).
21. Aarts, D.G.A.L., Lekkerkerker, H.N.W., Guo, H., Wegdam, G.H., and Bonn, D. "Hydrodynamics of droplet coalescence", *Phys. Rev. Lett.*, **95**, 164503 (2005).
22. Thoroddsen, S.T., Takehara, K., and Etoh, T.G. "The coalescence speed of a pendent and a sessile drop", *J. Fluid Mech.*, **527**, pp. 85-114 (2005).
23. Wu, M., Cubaud T., and Ho, C.M. "Scaling law in liquid drop coalescence driven by surface tension", *Phys. Fluids*, **16**, L51-L54 (2004).
24. Duchemin, L., Eggers, J., and Josserand, C. "Inviscid coalescence of drops", *J. Fluid Mech.*, **487**, pp. 167-178 (2003).
25. Ghosh, P. and Juve kar, V.A. "Analysis of the drop rest phenomenon", Chem. *Eng. Res. Design*, **80**(7), pp. 715-728 (2002).
26. Eggers, J., Lister, J.R., and Stone, H.A. "Coalescence of liquid drops", *J. Fluid Mech.*, **401**, pp. 293-310 (1999).
27. Amaya-Bower, L. and Lee, T. "Single bubble rising dynamics for moderate Reynolds number using lattice Boltzmann method", *Computers & Fluids*, **39**(7), pp. 1191-1207 (2010).
28. Stover, L.R., Tobias, C.W., and Denn, M.M. "Bubble coalescence dynamics", *AIChE Journal*, **43**, pp. 2385-2392 (1997).
29. Egan, E.W. and Tobias, C.W. "Measurement of interfacial re-equilibration during hydrogen bubble coalescence", *J. Electrochem. Soc.*, **141**, pp. 1118-1126 (1994).
30. Chaudhari, R.V. and Hofmann, H. "Coalescence of gas bubbles in liquids", *Rev. Chem. Eng.*, **10**, pp. 131-191 (1994).
31. Oolman, T.O. and Blanch, H.W. "Bubble coalescence in stagnant liquids", *Chem. Eng. Commun.*, **43**, pp. 237-261 (1986).
32. Hirt, C.W. and Nichols, B.D. "Volume of fluid (VOF) method for the dynamics of free boundaries", *J. Comp. Phys.*, **39**, pp. 201-225 (1982).
33. Bhaga, D. and Weber, M.E. "In-line interaction of a pair of bubbles in a viscous liquid", *Chem. Eng. Sci.*, **35**, pp. 2467-2474 (1980).
34. Narayanan, S., Goossens, H.J. and Kossen, N.W.F. "Coalescence of two bubbles rising in line at low Reynolds numbers", *Chem. Eng. Sci.*, **29**, pp. 2071-2082 (1974).
35. Amiri Rad, E. "Evaluation the radius dependency of surface tension in nano-droplets by a diffuse-interface lattice boltzmann", *Progress in Computational Fluid Dynamics An International Journal*, **17**(4), pp. 232-238 (2017).

36. Amiri Rad, E. and Salimi, M. "Investigating the effects of shear rate on the collapse time in a gas-liquid system by lattice Boltzmann", *Meccanica*, **52**(4-5), pp. 915-924 (2016)

37. Amiri Rad, E. "Control of droplet collapse during coarsening process by imposing shear flow: A lattice Boltzmann simulation", *Meccanica*, **50**(4), pp. 995-1001 (2015).

38. Amiri Rad, E. "Investigation the effects of shear rate on stationary droplets coalescence by lattice Boltzmann", *Meccanica*, **49**(6), pp. 1457-1467 (2014).

39. Amiri Rad, E. "Coalescence of two at-rest equal-sized drops in static vapor of the same material: A lattice Boltzmann approach", *J. Mech. Sci. Technol.*, **28**(9), pp. 3597-3603 (2014).

40. Dupuis, A. and Yeomans, J.M. "Modeling droplets on superhydrophobic surfaces: equilibrium states and transitions", *Langmuir.*, **21**, pp. 2624-2629 (2005).

41. Briant, A.J., Wagner, A.J., and Yeomans, J.M. "Lattice Boltzmann simulations of contact line motion. I. Liquid-gas systems", *Phys. Rev. E.*, **69**, 031602 (2004).

42. Swift, M.R., Osborn, W.R., and Yeomans, J.M. "Lattice Boltzmann simulation of nonideal fluids", *Phys. Rev. Lett.*, **75**, pp. 830-833 (1995).

43. Swift, M.R., Orlandini, E., Osborn, W.R., and Yeomans, J.M. "Lattice Boltzmann simulations of liquid-gas and binary fluid systems.", *Phys. Rev. E.*, **54**, pp. 5041-5052 (1996).

44. Hou, S., Zou, Q., Chen, S., Doolen, G. and Cogley, A.C. "Simulation of cavity flow by the lattice Boltzmann method", *J. Comput. Phys.*, **118**, pp. 329-347 (1995).

45. Shan, X. and Chen, H. "Simulation of nonideal gases and liquid-gas phase transitions by the lattice Boltzmann equation", *Phys. Rev. E.*, **49**, pp. 2941-2948 (1994).

46. Succi, S. "The Lattice Boltzmann Equation for Fluid Dynamics and Beyond", Oxford University Press (2001).

47. Holdych, D.J., Rovas, D., Georgiadis, J.G. and Buckius, R.O. "An improved hydrodynamics formulation for multiphase flow lattice-Boltzmann models", *Int. J. Mod. Phys.*, **C9**, pp. 1393-1404 (1998).

48. Evans, R. "The nature of the liquid-vapour interface and other topics in the statistical mechanics of non-uniform, classical fluids", *Adv. Phys.*, **28**, pp. 143-200 (1979).

49. Landau, L.D. and Lifshitz, E.M. *Statistical Physics*, Pergamon Press (1958).

50. Jamet, D., Torres, D. and Brackbill, J.U. "On the theory and computation of surface tension: The elimination of parasitic currents through energy conservation in the second-gradient method", *Journal of Computational Physics*, **182**, pp. 262-276 (2002).

Biography

Ehsan Amiri Rad received the BSc degree in Mechanical Engineering from Iran University of Science and Technology in 2005. Then, he received MSc degree in 2007 and PhD degree in 2011, in Energy Conversion, from Ferdowsi University of Mashhad, Iran. Currently, he is an Assistant Professor at Hakim Sabzevari University. He has published more than 30 papers in journals and international conference proceedings.